CliffDelineaTool v1.2.0: an algorithm for identifying coastal cliff base and top positions

Zuzanna M. Swirad, Adam P. Young

Scripps Institution of Oceanography, University of California San Diego, 9500 Gilman Dr., La Jolla, CA 92093, USA

5 *Correspondence to:* Zuzanna M. Swirad (zswirad@ucsd.edu)

Abstract. Correct quantification of coastal cliff erosion requires accurate delineation of the cliff face bounded by the cliff top and base lines. Manual mapping is time consuming and relies on mapper's decisions and skills. Existing algorithms are generally site specific and may be less suitable for areas with diverse cross-shore cliff geometry. Here we describe *CliffDelineaTool* (v1.2.0), a MATLAB/Python-based algorithm that identifies cliff base and top positions 10 on complex cliffs using cross-shore transects extracted from digital elevation models. Testing on four 750-1200 m cliffed coastlines shows that the model performance is comparable to manual mapping and provides some advantages over existing methods but provides poor results for cliff sections with ambiguous cliff top edges. The results can form the basis for a range of analyses including coastal inventories, erosion measurements, spatio-temporal erosion trends, and coastline evolution modelling.

1 Introduction

15

Correct quantification of cliff erosion for scientific and management purposes requires accurate delineation of coastal cliff faces. Cliff base and top positions are often digitized manually on georeferenced maps, aerial photographs, ortho-photographs, and digital elevation models (DEMs) (e.g. Dornbusch et al., 2008; Hapke et al., 2009; Brooks et al., 2012; Orviku et al., 2013; Swirad et al., 2017; Young, 2018). However, manual mapping is subject to the mapper's 20 decisions and skills (Moore, 2000). The lack of uniform definitions for a cliff base and top leads to further inconsistencies. Payo et al. (2018) suggested that for consistency, the mapping should be performed at the same time for the entire dataset, and by one mapper. However, this becomes problematic for multi-temporal studies, and those that build on previous efforts.

While manual digitization may be necessary when using cartographic sources, DEMs provide an opportunity to map 25 the cliff base and top programmatically as these features are characterized by local changes in slope (Liu et al., 2009). Preference of manual over automated mapping, particularly for small (<km) areas of interest, may result from clear visual recognition of cliff base and top positions, and challenges with developing an algorithm that works for a range of cliff geometries outside the initial calibration dataset. However, automated cliff delineation increases objectivity and consistency, and decreases processing time, which is particularly useful for large-area high-resolution topographic 30 datasets (Swirad and Young, 2021).

Several studies used automated or semi-automated techniques to separate the cliff face from foreshore and/or hinterland. The studies vary in terms of local settings, spatial scale, available source datasets, and purpose. For instance, Alessio and Keller (2020) extracted the cliff base as a 3 m (NAVD88) elevation contour. Richter et al. (2013)

applied terrain filters (1st and 2nd derivative of elevation) sensitive to slope change to identify the cliff base line for a simple cliff morphology. Several authors identified cliff base positions as inflection points along cross-shore transects. Liu et al. (2009) identified cliff base and top points using transects combined with image segmentation, surface reconstruction, and edge detection on ortho-images. For relatively simple cliffs, Terefenko et al. (2019) identified the cliff base as the seaward-most location along the transects with at least 0.5 m vertical change over 1 m horizontal distance. Palaseanu-Lovejoy et al. (2016) and Payo et al. (2018) developed methods based on the 'distance-to-trendline' where cliff base and top positions are extracted along cross-shore transects by comparing transect elevations with elevations along a straight line between transect ends ('trendline'). Cliff base and top points were defined as locations along the transects with the largest vertical distance between the cliff profile and trendline, with the cliff base located below and cliff top above the trendline. Palaseanu-Lovejoy et al. (2016) manually adjusted transect lengths to ensure that the cliff was the most prominent topographic feature. Palaseanu-Lovejoy (2021) updated the model (*iBluff*, coded in R) to include automatic outlier removal using a moving window (Tukey, 1977). Payo et al. (2018) developed the C++ *CliffMetrics* algorithm (available also in SAGA GIS; Payo, 2020) where the distance-to-trendline method is combined with automated transect generation for coasts with complex alongshore geometry. Payo et al. (2018) used a constant transect length to reduce pre-processing time. Errors associated with using the distance-to-trendline method are addressed by calibrating the 'vertical tolerance', transect length parameters, and manual quality control (Payo et al., 2018). *CliffMetrics* performs well for simple cross-shore cliff morphology, but it is less suitable for more complex cliff profiles, where rotational landslides, within-cliff flattening, roads, etc. are present (Swirad and Young, 2021).

Here, we build on previous models to develop a new MATLAB/Python-based algorithm, *CliffDelineaTool* (v1.2.0; Swirad, 2021) that identifies cliff base and top positions on cross-shore transects for a range of complex cliff geometries. The model parameters are calibrated using four cliff sections that encompass a range of geomorphic settings, and then tested on four different cliff sections with topography ranging from simple to complex. The results are compared to manually mapped cliff lines, the distance-to-trendline method, and *CliffMetrics* using default parameters.

2 Methods

2.1 *CliffDelineaTool* workflow

The model (Figure 1) uses eight user-defined parameters (Table 1) and an input text file containing rows of point ID, transect ID, distance from the seaward end of the transect, and elevation (Swirad et al., 2016). A single input file includes multiple ordered transects representing an entire coastal section.

Table 1. *CliffDelineaTool* user-defined parameters, and values optimized for the calibration coastal sections (areas of interest (AOIs) #1-4) and used to validate the model (AOIs #5-8).

Parameter	Description	Calibration				Validation			
		AOI #1	AOI #2	AOI #3	AOI #4	AOI #5	AOI #6	AOI #7	AOI #8
MaxBaseElev	Maximum elevation of the cliff base (m, NAVD88)	5	9	5	5	5	5	7	5
NVert	Number of consecutive points to define local scale	20	20	30	30	20	20	20	20
BaseSea	Maximum seaward slope angle at the cliff base (°)	12	13	9	15	20	20	20	15
BaseLand	Minimum landward slope angle at the cliff base (°)	34	4	6	29	30	20	30	20
TopSea	Minimum seaward slope angle at the cliff top (°)	39	32	18	14	30	25	30	40
TopLand	Maximum landward slope angle at the cliff top (°)	14	8	10	19	10	25	20	35
PropConvex	Threshold parameter for stage 2 cliff top replacement	n/a	0.4	0.1	0.6	0.2	0.8	0.5	0.5
SmoothWindow	Moving window size for cross-shore location smoothing (number of transects)	8	4	13	14	10	5	5	25

SET UP THE ALGORITHM

Load the file

Set parameter values (Table 1)

Identify columns of cross-shore distance and elevation

PREPARE TRANSECTS

Fill elevation data gaps

Calculate local slope angles

Limit transects landwards to the highest point + *NVert*

Create trendline #1 (line connecting transect ends)

Calculate vertical distance between cliff profile and trendline #1

IDENTIFY CLIFF BASE

Identify potential cliff base locations (elevation - trendline #1 < 0, > MaxBaseElev, < BaseSea, > BaseLand)

Select cliff base location (potential cliff base with max vertical distance between trendline #1 and elevation)

Cliff Top Stage 1: INITIAL CLIFF TOP

Create trendline #2 (line connecting cliff base and landward transect end)

Identify potential cliff top locations (elevation - trendline #2 > 0, > *TopSea*, < *TopLand*)

Select cliff top location (potential cliff top with max vertical distance between trendline #2 and elevation)

Cliff Top Stage 2: SHIFT CLIFF TOP LANDWARD?

Are there alternative potential cliff top locations > NVert landwards from the stage 1 cliff top?

YES
Vertical distance between the elevation and trendline #2 > PropConvex × that of the stage 1 cliff top?

NO
Retain stage 1 cliff top

YES
Point located above trendline #3?

NO
Retain stage 1 cliff top

YES
Select cliff top with largest vertical distance from trendline #2

NO
Retain stage 1 cliff top

Cliff Top Stage 3: REMOVE ALONGSHORE CLIFF TOP OUTLIERS

Define smoothed cliff top using median alongshore moving window (*SmoothWindow*)

Find cross-shore difference between cliff top and smoothed cliff top

Flag transects with outliers (standardized residual > 2)

Find potential cliff top closest to the smoothed cliff top location

Is its standardized residual > 2?

YES
Remove cliff top location; transect has no modelled cliff top ('skipped transect')

NO
Replace modelled cliff top

Figure 1. *CliffDelineaTool* **workflow and the three cliff top processing stages. Calibrated parameters** *NVert, MaxBaseElev, BaseSea, BaseLand, TopSea, TopLand, PropConvex, SmoothWindow* **are defined in Table 1.**

Processing is performed on a transect-by-transect basis. Transect elevation gaps are filled through extrapolation (transect peripheries) and linear interpolation (interior sections). For each point, local seaward and landward slope angles are calculated as an average slope between the point and a user-defined number of adjacent points called the *NVert* parameter. The *NVert* value is used at various stages of the model workflow to determine local spatial relationships between points (Swirad and Rees, 2015). To remove unnecessary inland points, the landward transect end is set to *NVert* points landward of the highest elevation. Next, a straight line ('trendline #1') is created by connecting transect ends (Figure 2a; after Payo et al., 2018).
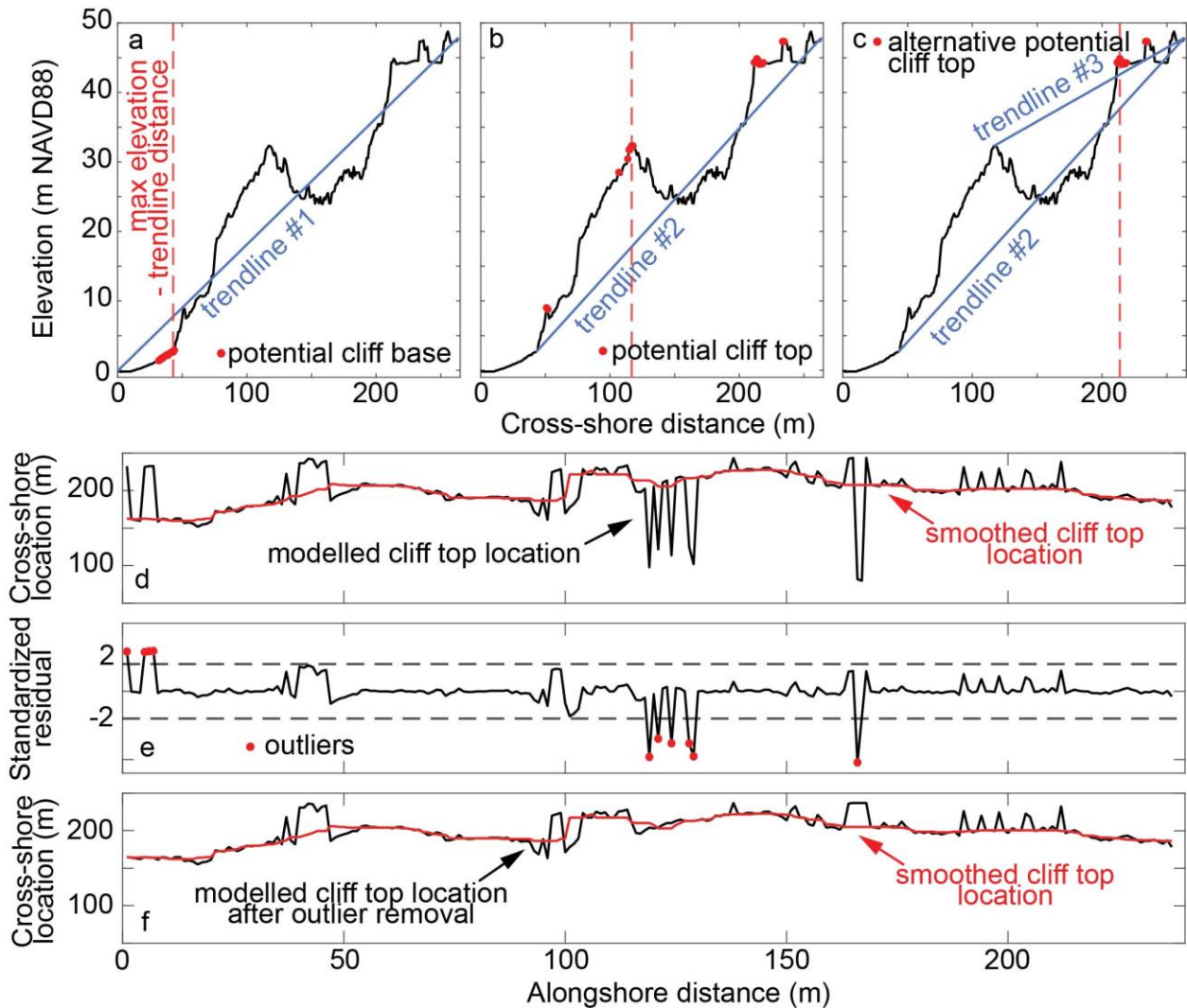
Figure 2. Example identification of cliff base and top positions (transect #123 of AOI #3; see Figure 3c for topography and oblique photograph): a) potential cliff base positions and the point with the largest distance from trendline #1; b) potential cliff top positions and the point with the largest distance from trendline #2 (stage 1); c) alternative potential cliff top positions in case of complex cross-shore profile and the point with the largest distance from trendline #2 (stage 2). Identification and removal of alongshore cliff top outliers (stage 3) – alongshore distribution of d) stage 2 modelled and smoothed cliff top; e) standardized residuals between smoothed and stage 2 modelled cliff top; f) stage 3 modelled cliff top with outliers removed. Note the vertical exaggeration in a-c and horizontal exaggeration in d-f.

Potential cliff base locations are below trendline #1 and fulfill user-defined criteria of maximum elevation of the cliff base (*MaxBaseElev*), maximum local seaward slope (*BaseSea*) and minimum local landward slope (*BaseLand*). These

criteria eliminate physically invalid cliff base elevations and ensure finding inflection points (concavities) at the full transect (relationship to the trendline) and local (seaward and landward slopes) levels. From the set of potential cliff base locations, the point with the largest vertical distance from the trendline is selected to represent the cliff base following Palaseanu-Lovejoy et al. (2016) and Payo et al. (2018) (Figure 2a). If no points fulfill the criteria, the transect is skipped at this stage.

Cliff top identification consists of three stages (Figure 1). In stage 1, trendline #2 is created by connecting the modelled cliff base with the landward end of the transect (Figure 2b). Potential cliff top locations are located above trendline #2 and fulfill user-defined criteria of minimum local seaward slope (*TopSea*) and maximum local landward slope (*TopLand*) defining local convexities. From the set of potential cliff top locations, the point with the largest vertical distance from trendline #2 is selected to represent the cliff top following Palaseanu-Lovejoy et al. (2016) and Payo et al. (2018) (Figure 2b). If no points along the transect fulfill the criteria, the transect is skipped and has no explicitly modelled cliff top.

In some locations with complex cliff face profiles, such as rotational landslides or mid-cliff roads, a local flattening within the cliff face may exist and cause an incorrect cliff top selection. To account for these situations, in stage 2 the model checks if any alternative potential cliff top exists landwards of the initial cliff top location identified in stage 1. Alternative potential cliff top positions located closer than *NVert* points from the initial top are rejected to ignore points that are likely part of the same convex section. Alternative positions must also be located above trendline #3 (a line from the initial cliff top to the landward transect end, Figure 2c), and greater than *PropConvex* (values between 0 and 1) multiplied by the elevation difference between the initial cliff top and trendline #2. For example, if *PropConvex* = 0.5 and the initial cliff elevation is 4 m above trendline #2, potential cliff top locations must be >2 m (0.5 × 4 m) above trendline #2. If alternative positions exist, the initial top is re-located to the point with the largest vertical distance from trendline #2 (Figure 2c). Otherwise, the initial cliff top is retained.

In stage 3, cliff top outliers are identified by comparing the cross-shore location to an alongshore smoothed cliff line, created from the median of an alongshore moving window (*SmoothWindow)* (Figure 2d). Residuals are calculated as a distance between the smoothed and modelled cross-shore locations. Transects with standardized residuals (residual divided by residual standard deviation) >2 are flagged as outliers (Figure 2e) and re-examined to identify new potential cliff top locations. If the standardized residual of the potential cliff top closest to the smoothed cross-shore location <2, it replaces the previously modelled top. Otherwise, the transect has no explicitly modelled cliff top (Figure 2f).

2.2 Model development

2.2.1 *CliffDelineaTool* calibration

To optimize user-defined parameters (Table 1), four calibration coastal cliff sections in California (areas of interest (AOIs) #1-4) were selected spanning 650-1200 m alongshore that encompass a range of geomorphic settings (Table 2; Figure 3a-d). Topographic information for each AOI was derived from 1 m DEMs created from a 2016 airborne LiDAR dataset (Swirad and Young, 2021).

Table 2. Characteristics of the areas of interest (AOIs) used to calibrate *CliffDelineaTool*. Average values are represented by mean ± standard deviation.

	AOI #1	AOI #2	AOI #3	AOI #4
Geographic location	34°28'15.54''N 120°13'8.30''W	33°18'49.31''N 117°29'7.61''W	33°20'47.17''N 117°31'20.70''W	35°57'24.90''N 121°28'57.90''W
Alongshore extent (m)	700	965	1180	655
Number of transects	141	194	237	132
Cross-shore extent (m)	87	159	264	249
Average cross-shore cliff extent (m)	23 ± 6	29 ± 15	153 ± 22	76 ± 32
Average cliff base elevation (m, NAVD88)	2.7 ± 0.4	6.7 ± 0.7	3.5 ± 0.7	4.3 ± 0.8
Average cliff height (m)	26 ± 2	23 ± 1	42 ± 2	60 ± 10
Average foreshore slope (°)	5.4 ± 5.4	5.7 ± 5.7	5.6 ± 3.6	7.1 ± 8.7
Average cliff slope (°)	47 ± 12	43 ± 18	28 ± 15	46 ± 13
Average hinterland slope (°)	10 ± 11	7.1 ± 10	16 ± 15	26 ± 17
Morphology	Cliff is the unique slope, beach and hinterland are planar, cliff top has a near-straight shape	Back beach berm, gullies that intersect the cliff top, complex cliff top line	Rotational landslides resulting in within-cliff flattening, vegetation, beach cusps, road within cliff face	Rocky foreshore, road adjacent to the cliff, sloping hinterland, gullies

7
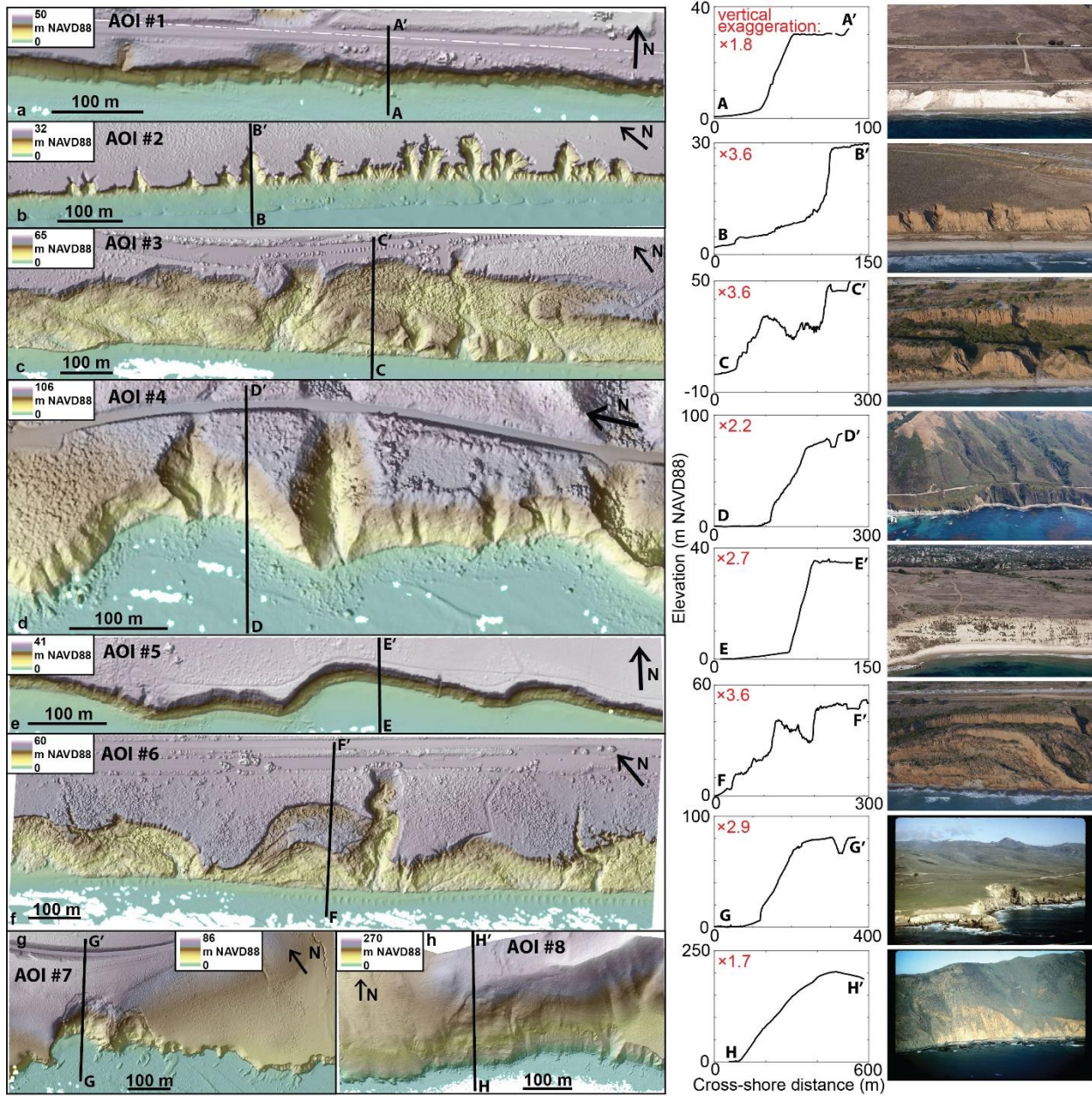
Figure 3. Areas of Interest (AOIs) used to calibrate (a-d) and validate (e-h) *CliffDelineaTool*. Vertical exaggeration is labelled in red for profiles. Photographs copyright © 2002-2021 Kenneth & Gabrielle Adelman, California Coastal Records Project, www.Californiacoastline.org.

Parallel calibration transects generated with ArcGIS tools were spaced 5 m alongshore to capture meso-scale details of alongshore cliff geometry and sampled at 1 m cross-shore resolution. Points representing 'true' cliff base and top locations were visually selected for each transect. The *CliffDelineaTool* results were compared with the distance-to-trendline method (Palaseanu-Lovejoy et al., 2016) and *CliffMetrics* (SAGA GIS version; Payo, 2020) using input parameters (seaward transect end points, transect length, and no transect smoothing) to match the same cross shore transects used for *CliffDelineaTool* and the default vertical tolerance of 0.5. Maximum cliff base elevation (*MaxBaseElev*) was subjectively set to 5 m (NAVD88) for AOIs #1, #3, and #4, and 9 m (NAVD88) for AOI #2 based

8

on DEM inspection (Figure 3, Table 2). The remaining seven parameters were calibrated to minimize root mean squared error (RMS) between true and modelled cliff base and top positions while not skipping too many transects.

135   *NVert* and threshold slope angles (*BaseSea*, *BaseLand*, *TopSea* and *TopLand*) were calibrated using the characteristics of the true cliff base and top locations. Slope angles were calculated for a range of *NVert* values (Table 2). Local slope angle distributions were summarized in statistical terms (Figure 4), and outliers were defined as points greater than q_3 + *1.5 × (q_3 - q_1)* or less than q_1 - *1.5 × (q_3 - q_1),* where q_1 and q_3 are the 25th and 75th percentiles (red pluses in Figure 4; Tukey, 1977). *NVert* = 20 was selected for AOIs #1-2 and *NVert* = 30 was selected for AOIs #3-4 to minimize the

140   number of outliers while maintaining a relatively narrow and normal slope angle distribution. Threshold slope angles were picked as minimum or maximum values excluding outliers (q_3 + *1.5 × (q_3 - q_1)* or q_1 - *1.5 × (q_3 - q_1)*); black whisker ends in Figure 4; Table 1).
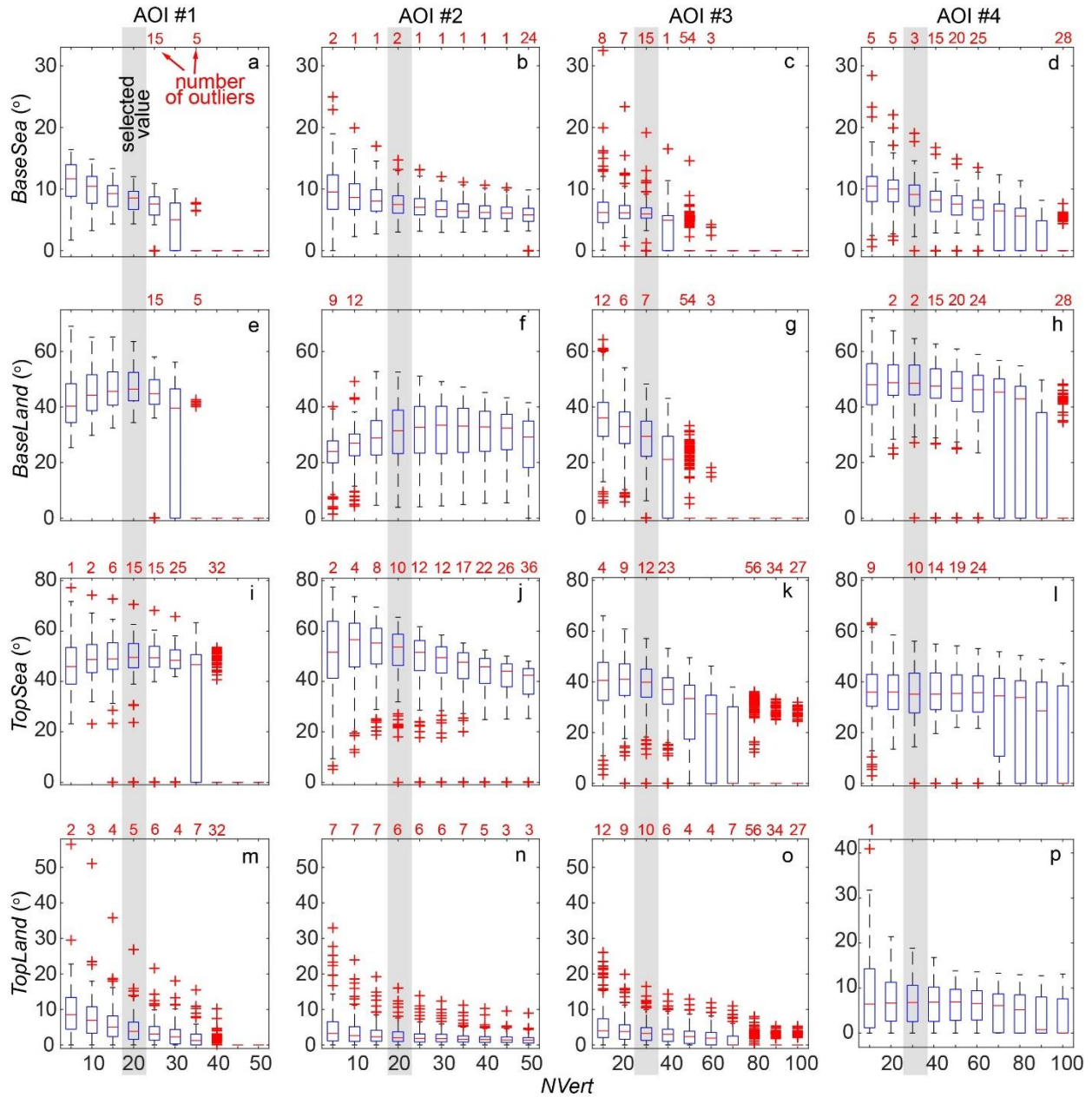
Figure 4. Distributions of the local seaward and landward slopes of true cliff base and top locations for varying *NVert* values. Boxplots include median (red bar), 25th (q_1) and 75th (q_3) percentiles (blue box), range excluding outliers (black whiskers) and outliers (red pluses). Outliers are defined as values greater than $q_3 + 1.5 \times (q_3 - q_1)$ or less than $q_1 - 1.5 \times (q_3 - q_1)$. Values in red located above the plots provide the number of outliers (if >0). Grey shadow indicates local slope distributions at selected *NVert* value.

Next, *CliffDelineaTool* checks for false cliff tops caused by a local flattening within the cliff face using *PropConvex* (stage 2 of the model, Figure 1). *PropConvex* was calibrated by inspecting the cliff top RMS for values ranging from 0.1 to 0.9 at 0.05 intervals (Figure 5a-d). For the simple cliff morphology of AOI #1, introducing *PropConvex* did not change the modelled cliff top locations, but it did decrease the RMS for more complex AOIs #2-4 (Figure 5a-d; Table 1). Next, cliff top outliers were identified. Optimal *SmoothWindow* was selected by comparing moving window ranging from 1 to 20 alongshore transects for each AOI to minimize RMS and number of skipped transects (Figure

10

155 5e-h; Table 1). The modelled cliff base and top locations were converted to polylines using ArcGIS and intersected with transects to define cliff base and top locations on skipped transects. Overall, these steps improved automated cliff mapping performance for the more complex cliff sections and usually exhibited lower RMS compared to the distance-to-trendline method and *CliffMetrics* (Table 3; Figure 6).
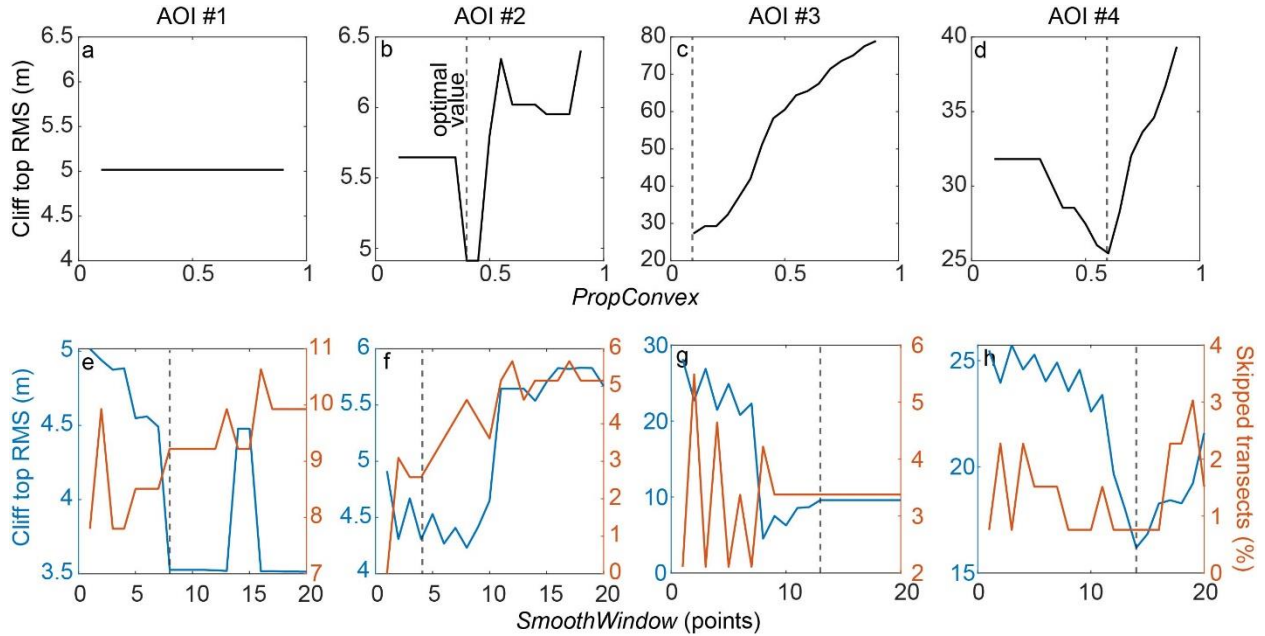
160 **Figure 5. Calibration of *PropConvex* (testing from 0.1 to 0.9 at 0.05 interval) (a-d) and *SmoothWindow* (testing from 1 to 20 transects) (e-h). Vertical dashed lines represent the optimal values (Table 1).**

Table 3. Performance of *CliffDelineaTool* at various stages, the distance-to-trendline method and *CliffMetrics* (Payo, 2020).

AOI	Error metric	CliffDelineaTool				Distance-to-trendline	CliffMetrics (default paramters)
		Stage 1	Stage 2	Stage 3	Stage 3 including skipped transects		
#1	Skipped cliff base points (%)	0	0	0	0	0	0
	Cliff base RMS (m)	0.3	0.3	0.3	0.3	0.4	0.6
	Skipped cliff top points (%)	7.8	7.8	9.2	0	0	0
	Cliff top RMS (m)	5.0	5.0	3.6	6.1	5.0	4.9
#2	Skipped cliff base points (%)	0	0	0	0	0	0
	Cliff base RMS (m)	5.9	5.9	5.9	5.9	14	12
	Skipped cliff top points (%)	0	0	2.6	0	0	0
	Cliff top RMS (m)	6.7	4.9	4.4	4.9	5.8	5.8
#3	Skipped cliff base points (%)	2.1	2.1	2.1	0	0	0
	Cliff base RMS (m)	5.4	5.4	5.4	5.3	74	70
	Skipped cliff top points (%)	2.1	2.1	2.1	0	0	0
	Cliff top RMS (m)	83	28	9.7	10	74	73
#4	Skipped cliff base points (%)	0.8	0.8	0.8	0	0	0
	Cliff base RMS (m)	1.7	1.7	1.7	2.0	31	11
	Skipped cliff top points (%)	0.8	0.8	0.8	0	0	0
	Cliff top RMS (m)	40	26	16	16	29	28
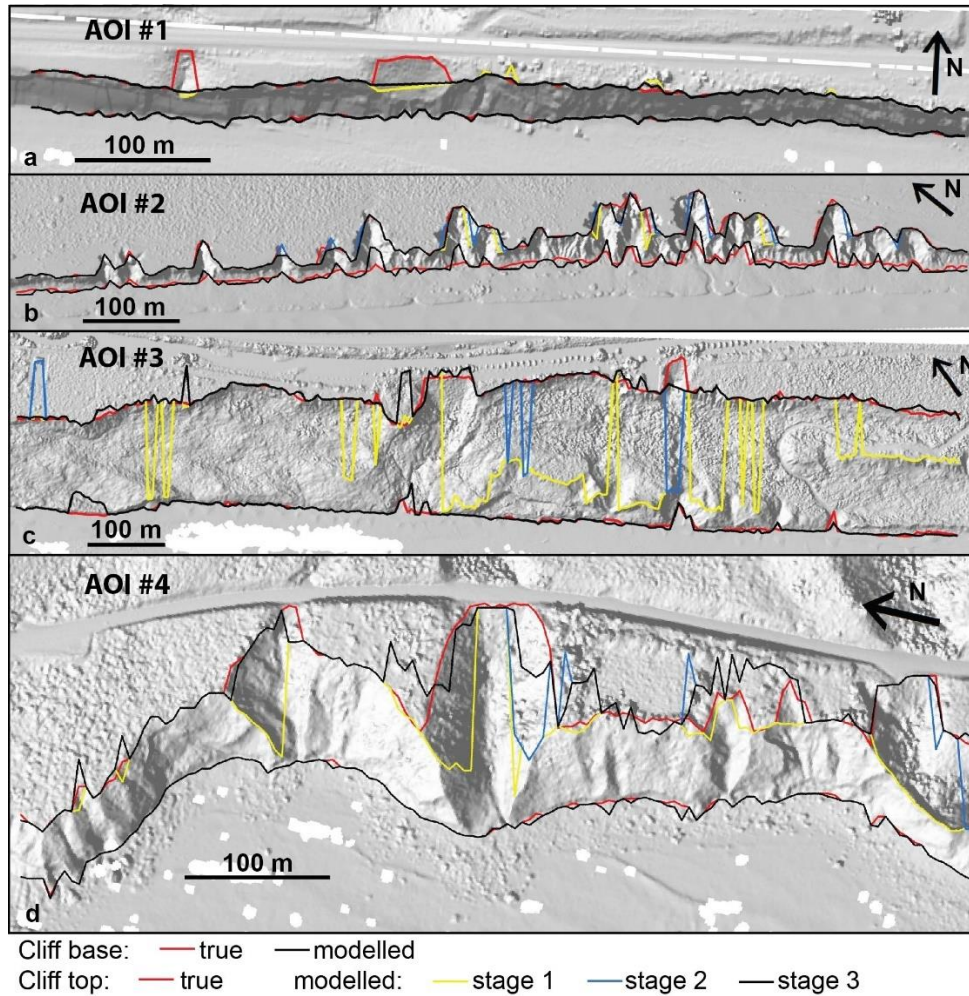
Figure 6. Location of the cliff base and top at various stages of the *CliffDelineaTool* calibration.

165 ### 2.2.2 *CliffDelineaTool* evaluation

Ten geoscientists manually digitized the cliff base and top for four different sections of the California coastline (AOIs #5-8) with diverse morphology using 1 m resolution DEMs and hillshade maps (Table 4; Figure 3e-h). The 'true' cliff base and top positions were defined as the median of the manually mapped positions.

12

	AOI #5	AOI #6	AOI #7	AOI #8
Geographic location	34°25'6.44''N 119°47'49.20''W	33°21'19.13''N 117°32'3.34''W	34°33'36.12''N 120°37'49.53''W	34°54'6.71''N 120°39'36.70''W
Alongshore extent (m)	845	1195	745	1075
Number of transects	170	240	150	216
Cross-shore extent (m)	134	309	366	650
Average cross-shore cliff extent (m)	26 ± 4	101 ± 42	49 ± 40	158 ± 56
Average cliff base elevation (m, NAVD88)	3.3 ± 0.6	4.9 ± 1.0	3.9 ± 2.3	3.6 ± 1.9
Average cliff height (m)	31 ± 3	34 ± 4	38 ± 17	105 ± 35
Average foreshore slope (°)	4.4 ± 4.3	7.4 ± 7.2	7.5 ± 8.5	6.8 ± 8.6
Average cliff slope (°)	50 ± 10	30 ± 17	38 ± 17	36 ± 8.2
Average hinterland slope (°)	6.9 ± 7.3	17 ± 15	11 ± 9.2	22 ± 10
Morphology	Cliff is the unique slope, beach and hinterland are planar, cliff top has a near-straight shape	Rotational landslides resulting in within-cliff flattening, trees, beach cusps, gullies that intersect the cliff top	Plunging cliff, foreshore rocks, road adjacent to the cliff, sloping hinterland	Steep hinterland, cliff is part of a mountain slope, multiple superposed landslides

CliffDelineaTool, the distance-to-trendline method, and *CliffMetrics* were applied on the four test sections (AOIs #5-8) and compared to the manually mapped cliff lines. For *CliffDelineaTool*, *NVert* was set at 20 because the test sections have the same 1 m DEM resolution as the calibration set. *MaxBaseElev* was set based on average cliff base elevation (Table 4). Remaining parameters values (*BaseSea*, *BaseLand*, *TopSea*, *TopLand*, *PropConvex* and *SmoothWindow*) were selected based on average foreshore, cliff and hinterland slopes (Table 4), and visual assessment on initial model runs (Table 1). RMS between true and modelled cliff base and top locations was used to assess model performance on all transects (including skipped transects).

3 Results

Consistency of the manual, and performance of the automated cliff mapping varied between the four evaluation AOIs. The simple cliff geometry and unambiguous location of the cliff base and top of AOI #5 resulted in low (≤2.7 m) RMS for all mapping methods (Table 5; Figure 7a-b). In general, cliff base locations were more consistent between manual mappers and *CliffDelineaTool* compared to the cliff top. The distance-to-trendline method had relatively high (>>10 m) cliff base RMS for all three complex AOIs (#6-8), sometimes placing the cliff base on the upper cliff face or hinterland (B in Figure 7d). Using default parameters, *CliffMetrics* generally performed better than the distance-to-trendline method, but had higher RMS compared to *CliffDelineaTool*. *CliffDelineaTool* (RMS = 1.1-8.2 m) and manual mapping (RMS = 0.7-11 m) gave comparable cliff base detection results. For AOI #6 the distance-to-trendline method and *CliffMetrics* sometimes placed cliff base at beach cusps (C in Figure 7d). For complex AOIs #6-8, manual and automated cliff top positions were varied (RMS = 2.9-214 m). In AOI #6 one mapper (#2) selected the head scarp of an interior landslide as the cliff top about 100 m from the cliff top selected by all other mappers (A in Figure 7c). However, the models also picked sections of the landslide head scarp (D in Figure 7d). In AOI #7 two mappers interpreted an elevated section between two separate landslide scars as cliff top (E in Figure 7e), differing from most other mappers and both models that opted for a simpler cliff top shape (Figure 7e-f). The cliff top position was the

most diverse for AOI #8, with mappers' interpretation ranging from the top of the coastal mountain slope (F in Figure 7g) to the mid-slope (G in Figure 7g), and tops of interior cliff face landslide scars (H in Figure 7g). *CliffDelineaTool* gave inconsistent results, while the distance-to-trendline method and *CliffMetrics* placed the cliff top at the top of the mountain slope (Figure 7h).

Table 5. RMS between the true (median of manually mapped), individual manual mapping and modelled cliff base and top positions.

	AOI #5		AOI #6		AOI #7		AOI #8	
	base	top	base	top	base	top	base	top
Mapper #1	0.9	1.1	2.5	8.1	11	2.9	3.6	174
Mapper #2	1.0	1.5	4.3	28	3.6	6.8	3.0	79
Mapper #3	1.1	1.3	1.5	10	4.8	18	4.2	166
Mapper #4	0.8	1.7	1.2	7.5	1.8	5.3	2.9	116
Mapper #5	0.8	1.2	1.3	10	2.7	13	2.7	25
Mapper #6	1.4	1.3	4.3	9.0	6.6	21	5.8	111
Mapper #7	1.1	1.7	1.2	16	5.6	4.2	5.1	61
Mapper #8	1.0	1.5	1.6	11	3.5	4.1	3.7	169
Mapper #9	0.9	2.3	1.3	11	3.4	3.9	2.3	49
Mapper #10	0.7	1.9	2.7	13	5.2	5.4	2.5	17
Average of mappers	1.0	1.5	2.2	12	4.8	8.5	3.6	97
Distance-to-trendline	2.1	2.7	82	32	82	28	63	215
CliffMetrics (default parameters)	2.0	2.5	40	30	10	28	75	201
CliffDelineaTool	1.1	1.5	3.8	25	8.2	8.3	4.8	99
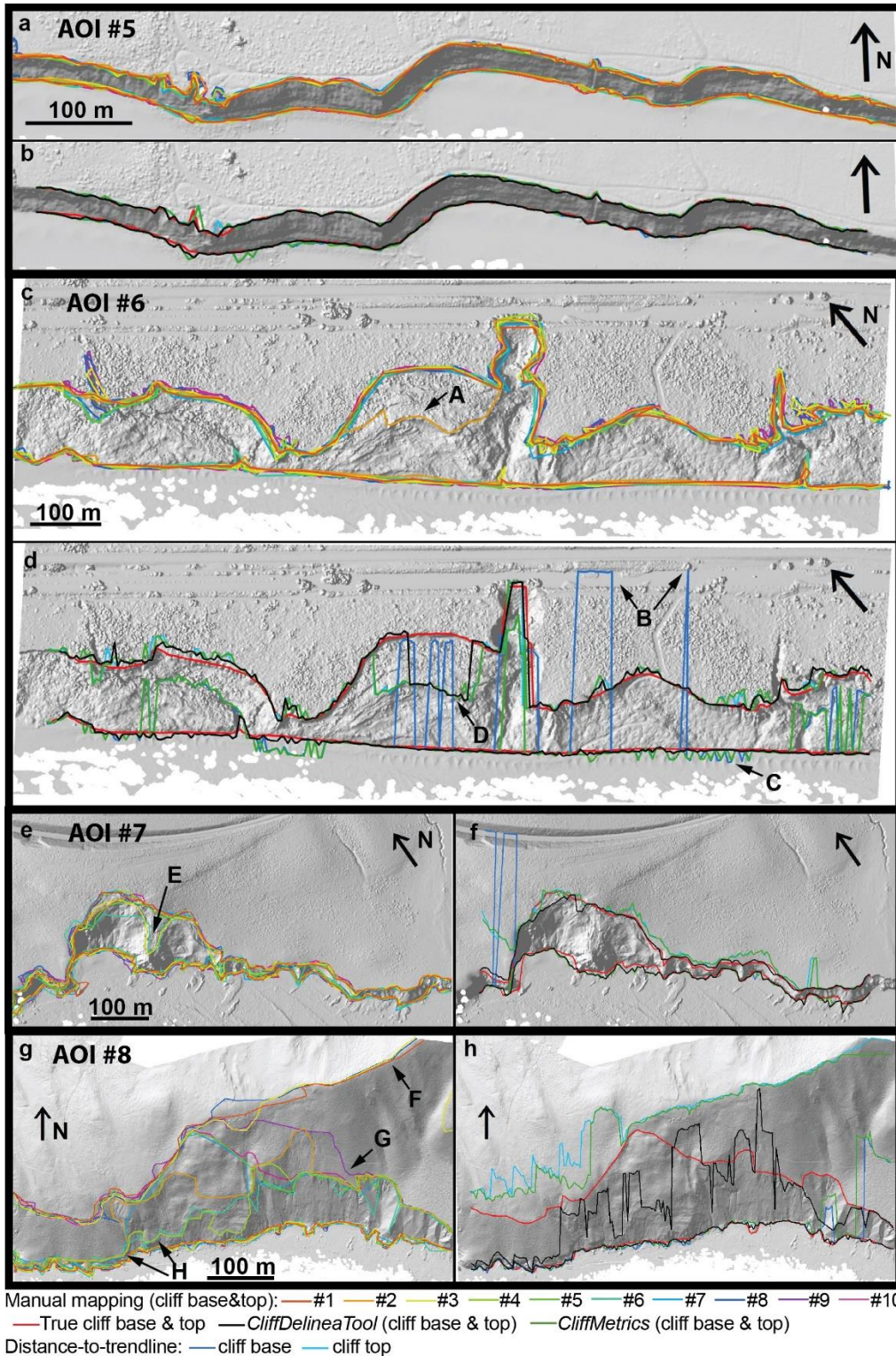
Figure 7. (a, c, e, g) Individual manually mapped and (b, d, f, h) median of manual mapping and modelled cliff base and top positions for AOIs #5-8. Locations A: pre-slide cliff top position interpreted as cliff top by mapper #2; B: cliff base placed in the hinterland by the distance-to-trendline method; C: beach cusps identified as cliff base by the distance-to-trendline method and *CliffMetrics*; D: interior cliff face location selected as cliff top by all models; E: elevated section between two landslide scars interpreted as cliff top by two mappers; F: top of the mountain slope interpreted as the cliff top; G: cliff top placed in the mid-slope; H: cliff top placed at the lower mountain slope.

4 Discussion

Acceptable model results depend on the purpose of cliff delineation. At the scale and resolution considered here, the model generally provided comparable results to manual mapping for diverse cliff morphology. Model performance generally correlates with the amount of inconsistency between manual mappers related to the cliff complexity. For example, in complex AOI #8 mean manual mapper and *CliffDelineaTool* RMS were both high (97 and 99 m, respectively). Conversely, for simple AOI #5, manual mapper and *CliffDelineaTool* RMS were both low (1.5 m both). The present model does not resolve the situations where a transect crosses the cliff top multiple times, and typically places the cliff top at the seaward-most crossing point (Figure 6b). Other model application issues include occasional treetop selection for cliff top positions (Figure 6c-d) when using non-bare-earth DEMs. Given these issues and high RMS in complex cliff sections we suggest that model outputs should be visually controlled (similar to Payo et al., 2018), and not used where the cliff top is very ambiguous such as AOI #8 with complex tall mountain slopes.

Unlike the models of Palaseanu-Lovejoy et al. (2016) and Payo et al. (2018), *CliffDelineaTool* does not generate transects. For this study, simple cross shore transects with 5 m alongshore spacing were defined manually for each AOI. The relatively short AOI alongshore sections permitted use of parallel transects (Swirad, 2021). However, for longer, more complex cliff sections varying transect orientation will improve results and could be generated with *CliffMetrics* (Payo et al., 2018).

We compared *CliffDelineaTool* to the distance-to-trendline method which forms basis of *iBluff* (Palaseanu-Lovejoy, 2021) and *CliffMetrics* (Payo et al., 2018). However, *iBluff* and *CliffMetrics* both include additional steps to improve results and correct erroneous cliff base and top positions. *iBluff* uses manual transect shortening during pre-processing, and outlier removal using smoothing window, similar to *CliffDelineaTool*. *CliffMetrics* uses manual quality control and iterative parameter selection (Payo et al., 2018). The *CliffMetrics* results presented here used default parameters and predefined transects to provide a direct comparison to *CliffDelineaTool*. However, one of the strengths of *CliffMetrics* includes the ability to quickly iterate parameter set up. Therefore, the results could be improved using iterative parameter selection and varying transect length and orientation.

For best performance, *CliffDelineaTool* should be calibrated to the user study section. The input parameters have a varied impact on model performance (Figure 6). *MaxBaseElev* is easily selected using a slightly conservative cliff base elevation estimated from the general site settings. The optimal *NVert* parameter depends on DEM resolution and cross-shore cliff extent. Calibration showed that in general the greater the *NVert* value the narrower the distribution of the four threshold slopes (*BaseSea*, *BaseLand*, *TopSea* and *TopLand*) and the higher the number of outliers. That relationship holds until *NVert* value (30 for AOI #1, 40 for #3 and 70 for #4, Figure 4) over which the q_1 - q_3 box becomes very wide or the distribution is dominated by outliers. Figure 8 shows the cliff top optimized for *NVert* values of 10, 20, 30, 40 and 50 for AOI #4. It suggests that during stage 2, low *NVert* value can cause incorrect cliff top section caused by minor protruding features such as vegetation (A in Figure 8), while higher value can inhibit correct stage 2 cliff top replacement (B in Figure 8). *TopLand* of 10-20° is generally appropriate when hinterland is planar or gently sloping but should be increased for cliffs with steeper inland areas. *BaseSea* and *BaseLand* are important for proper cliff base placement for coastal sections with back beach cusps and landslide deposits. *SmoothWindow* parameter depends on alongshore complexity of the coast, bay/headland sequence spacing, and their relation to

transect spacing. Model results are sensitive to *TopSea*, *PropConvex* and *SmoothWindow,* and testing various values on short sections of the study area with visual inspection can help identify optimal values (Figure 6).
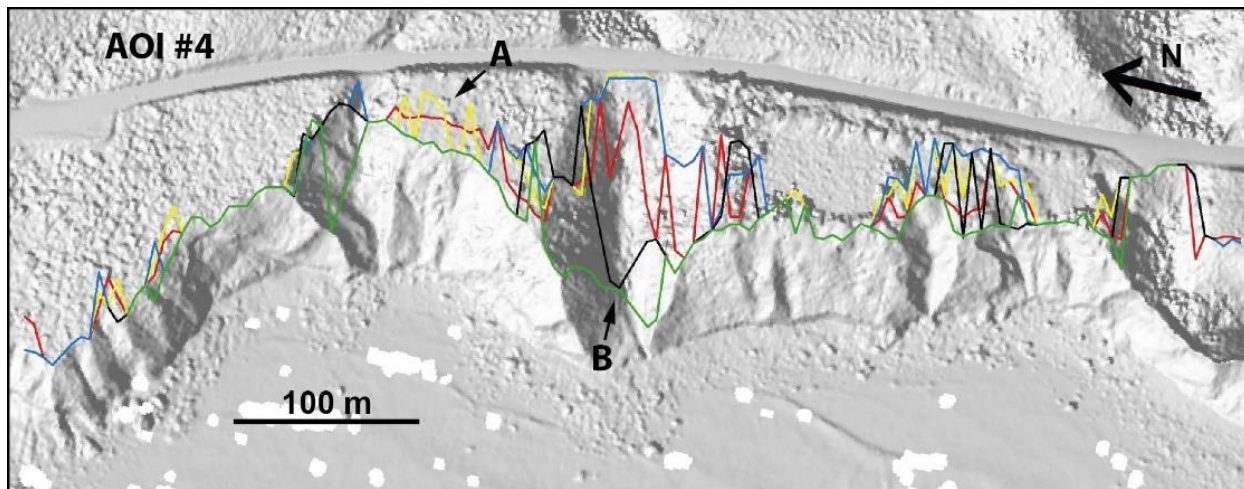
Figure 8. Location of the stage 2 cliff top after optimizing all parameters for *NVert* ranging 10-50. Location A: vegetation interpreted as cliff top for model runs with low *NVert* values. Location B: high *NVert* values can inhibit correct stage 2 cliff top replacement to locations further landward.

Two previous studies have successfully used parts of *CliffDelineaTool*. Swirad and Young (2021) used a modified version of *CliffDelineaTool* to automate mapping of cliff base and top positions along the California coast (1646 km). The modified version did not include stage 2 (shifting cliff top landwards for within-cliff flattening areas) and stage 3 (removal of outliers) but did include a Laplacian topographic filter (Richter et al., 2013). The automated results were visually inspected and some (10% of the cliff base and 29% of the cliff top positions) required manual modification to correct positions. Young et al. (2021) used the present *CliffDelineaTool* model to identify the cliff base in 155 0.25 m resolution DEMs along a 2.5 km coastal section at 1 m alongshore transect spacing. Quality control showed that cliff base misplacement was negligible, while the total processing time was ~30 min (Young et al., 2021). These studies demonstrate the tool's applicability for both large space and time datasets, and over a range of DEM resolutions.

5 Conclusions

Building on previous studies, we developed a new algorithm (*CliffDelineaTool*) to delineate coastal cliffs from DEMs. The model identifies cliff base and top positions along cross-shore transects using elevation and slope characteristics. It considers complex cliff morphology and removes alongshore cliff top outliers. *CliffDelineaTool* provides results comparable to manual mapping and improves cliff base and top identification for complex cross-profiles. The automated results have known errors and should be inspected visually. The method has been applied successfully on two large datasets (Swirad and Young, 2021; Young et al., 2021), greatly reducing processing time. With calibration and quality control *CliffDelineaTool* can be used on a wide variety of coastal setting facilitating a range of scientific and managerial applications but has limited application where the cliff top is ambiguous.

Code availability

CliffDelineaTool was initially coded in MATLAB R2019a. The source code, and the calibration and validation
270 datasets explored in this paper (DEMs, model input, true and modelled cliff base and top positions) are available at
https://zenodo.org/record/5724975 (Swirad, 2021). See https://github.com/zswirad/CliffDelineaTool (last access:
2021-11-24) for the latest version of the source code, Python version of the tool (*CliffDelineaToolPy*, v1.0.0) and user
instructions.

285 **References**

Alessio, P. and Keller, E. A.: Short-term patterns and processes of coastal cliff erosion in Santa Barbara, California,
Geomorphology, 353, 106994, doi: 10.1016/j.geomorph.2019.106994, 2020.

Brooks, S. M., Spencer, T. and Boreham, S.: Deriving mechanisms and thresholds for cliff retreat in soft-rock cliffs
under changing climates: Rapidly retreating cliffs of the Suffolk coast, UK, Geomorphology, 153–154, 48–60, doi:
290 10.1016/j.geomorph.2012.02.007, 2012.

Dornbusch, U., Robinson, D. A., Moses, C. A. and Williams, R. B., G.: Temporal and spatial variations of chalk cliff
retreat in East Sussex, 1873 to 2001, Marine Geology, 249, 271–282, doi: 10.1016/j.margeo.2007.12.005, 2008.

Hapke, C. J., Reid, D. and Richmond, B.: Rates and trends of coastal change in California and the regional behavior
of the beach and cliff system, J. Coast. Res, 25(3), 603–615, doi: 10.2112/08-1006.1, 2009.

295 Liu, J. K., Li, R., Deshpande, S., Niu, X. and Shih, T. Y.: Estimation of blufflines using topographic Lidar data and
orthoimages, Photogramm. Eng. Remote Sensing, 75(1), 69–79, 2009.

Moore, L. J.: Shoreline mapping techniques. J. Coast. Res., 16(1), 111–124, 2000.

Orviku, K., Tõnisson, H., Kont, A., Suuroja, S. and Anderson, A.: Retreat rate of cliffs and scarps with different
geological properties in various locations along the Estonian coast, J. Coast. Res., SI65, 552–557, doi: 10.2112/SI65-
300 094.1, 2013.

Palaseanu-Lovejoy, M.: iBluff - Geomorphic analysis of coastal bluffs/cliffs [code], https://doi.org/10.5066/P9HJ7QHD [https://code.usgs.gov/gmegsc/ibluff.git], 2021.

Palaseanu-Lovejoy, M., Danielson, J., Thatcher, C., Foxgrover, A., Barnard, P., Brock, J. and Young, A.: Automatic delineation of seacliff limits using lidar-derived high-resolution DEMs in Southern California, J. Coast. Res, SI76, 305   162–173, doi: 10.2112/SI76-014, 2016.

Payo, A., Jigena Antelo, B., Hurst, M., Palaseanu-Lovejoy, M., Williams, C., Jenkins, G., Lee, K., Favis-Mortlock, D., Barkwith, A. and Ellis, M. A.: Development of an automatic delineation of cliff top and toe on very irregular planform coastlines (CliffMetrics v1.0). Geosci. Model Dev., 11, 4317–4337, doi: 10.5194/gmd-11-4317-2018, 2018.

Payo, A.: Tool CliffMetrics. SAGA-GIS Tool Library Documentation (v7.9.0). http://www.saga-310   gis.org/saga_tool_doc/7.9.0/ta_cliffmetrics_0.html, 2020.

Richter, A., Faust, D. and Maas, H.-G.: Dune cliff erosion and beach width change at the northern and southern spits of Sylt detected with multi-temporal Lidar, Catena, 103, 103–111, doi: 10.1016/j.catena.2011.02.007, 2013.

Swirad, Z. M.: zswirad/CliffDelineaTool: Coastal cliff mapping algorithm with Py version and GMDD modifications (v1.2.0), Zenodo, doi: 10.5281/zenodo.5724975, 2021.

315   Swirad, Z. M., Migoń, P. and Strzelecki, M. C.: Rock control on the shape of coastal embayments of north-western Hornsund, Svalbard, Zeitschrift für Geomorphologie, 61(1), 11–28, doi: 10. 1127/zfg/2017/0403, 2017.

Swirad, Z. M. and Rees, W. G.: Geomorphometric analysis of a rocky coastline: an example from Hornsund, Svalbard, Int. J. Geogr. Inf. Sci.,29, 1694–1717, doi: 10.1080/13658816.2015.1061131, 2015.

Swirad, Z. M., Rosser, N. J., Brain, M. J. and Vann Jones, E. C.: What controls geometry of rocky coasts at the local 320   scale? J. Coast. Res, SI75, 612–616, doi: 10.2112/SI75-123.1, 2016.

Swirad, Z. M. and Young, A. P.: Automating coastal cliff erosion measurements from large-area LiDAR datasets in California, USA, Geomorphology, 389, 107799, doi: 10.1016/j.geomorph.2021.107799, 2021.

Terefenko, P., Paprotny, D., Giza, A., Morales-Nápoles, O., Kubicki, A. and Walczakiewicz, S.: Monitoring cliff erosion with LiDAR surveys and Bayesian network-based data analysis, Remote Sens., 11, 843, doi: 325   10.3390/rs11070843, 2019.

Tukey, J. W.: Exploratory data analysis, Addison-Wesley, Boston, USA, 1977.

Young, A. P.: Decadal-scale coastal cliff retreat in southern and central California. Geomorphology, 300, 164–175, doi: 10.1016/j.geomorph.2017.10.010, 2019.

Young, A. P., Guza, R. T., Matsumoto, H., Merrifield, M. A., O'Reilly, W. C. and Swirad, Z. M.: Three years of 330   weekly observations of coastal cliff erosion by waves and rainfall. Geomorphology, 375, 107545, doi: 10.1016/j.geomorph.2020.107545, 2021.